Original Article

Cinacalcet attenuated bone loss via inhibiting parathyroid hormone-induced endothelial-to-adipocyte transition in chronic kidney disease rats

Li-Hua Ni[1#], Ri-Ning Tang[1,2#], Cheng Yuan[3], Kai-Yun Song[1], Li-Ting Wang[1], Xiao-Liang Zhang[1], Lin-Li Lv[1], Bin Wang[1], Min Wu[1], Tao-Tao Tang[1], Zuo-Lin Li[1], Di Yin[1], Jing-Yuan Cao[1], Xiao-Chen Wang[1], Hong Liu[1], Qiang Chen[4], Bi-Cheng Liu[1]

[1]Institute of Nephrology, Zhongda Hospital, Southeast University School of Medicine, Nanjing 210009, China; [2]NanJing Lishui People's Hospital, Zhongda Hospital Lishui Branch, Nanjing 210009, China; [3]Department of Radiation and Medical Oncology, Zhongnan Hospital, Wuhan University, Wuhan 430071, China; [4]Biomechanics Laboratory, School of Biological Science and Medical Engineering, Southeast University, Nanjing 210096, China

Contributions: (I) Conception and design: LH Ni, RN Tang, BC Liu; (II) Administrative support: RN Tang, BC Liu; (III) Provision of study materials or patients: LH Ni, KY Song, RN Tang, BC Liu; (IV) Collection and assembly of data: LH Ni, Cheng Yuan, KY Song, RN Tang, BC Liu; (V) Data analysis and interpretation: LH Ni, KY Song, RN Tang, BC Liu, C Yuan; (VI) Manuscript writing: All authors; (VII) Final approval of manuscript: All authors.

[#]These authors contributed equally as co-first authors.

Correspondence to: Bi-Cheng Liu; Ri-Ning Tang. Institute of Nephrology, Zhongda Hospital, Southeast University School of Medicine, Nanjing 210009, China. Email: liubc64@163.com; tangrn77@163.com.

Background: Recently, cinacalcet (CINA) has been shown to be effective for attenuating bone loss in the treatment of secondary hyperparathyroidism (SHPT) in patients with chronic kidney disease (CKD), which might be associated with the reduction in serum parathyroid hormone (PTH) levels. However, the exact mechanism is largely unclear. Emerging studies have revealed that an increased number of bone marrow adipocytes (BMAs) are involved in bone loss and the endothelial-to-adipocyte transition via the endothelial-to-mesenchymal transition (EndMT) might play a key role in this pathological process. Here, we assessed whether CINA could attenuate bone loss via inhibiting endothelial-to-adipocyte transition in CKD rats.

Methods: A rat model of CKD was induced by adenine and a high phosphorus diet. CINA was orally administrated to CKD animals (10 mg/kg once a day). Dual energy X-ray absorptiometry, micro-computed tomography, bone histomorphometry, and bone mechanical tests were used to determine the skeletal changes. The bone marrow expression of EndMT markers was also examined. The effect of elevated PTH levels on the endothelial-to-adipocyte transition was studied in endothelial cells (ECs).

Results: Elevation of serum PTH levels, remarkable bone loss and increased numbers of BMAs were observed in rats with CKD compared with the controls, and these changes were attenuated after treatment with CINA. Furthermore, the CINA treatment abolished the upregulation of mesenchymal markers (FSP1 and α-SMA) and the downregulation of an endothelial marker (CD31) in bone tissues from rats with CKD. The serum PTH concentrations were correlated with the bone marrow protein levels of these EndMT-related proteins. An *in vitro* treatment in ECs demonstrated that PTH induced the EndMT in a concentration- and time-dependent manner. Accordingly, ECs treated with PTH exhibited adipogenic potential following growth in adipogenic culture medium.

Conclusions: Our study indicated CINA treatment attenuated bone loss in CKD rats, which might be associated with inhibiting PTH-induced endothelial-to-adipocyte transition in CKD rats.

Keywords: Chronic kidney disease (CKD); parathyroid hormone (PTH); osteoporosis; endothelial cells (ECs); adipocytes

Submitted Feb 03, 2019. Accepted for publication Jun 17, 2019.
doi: 10.21037/atm.2019.06.44
View this article at: http://dx.doi.org/10.21037/atm.2019.06.44

Introduction

Bone loss is a common complication of chronic kidney disease (CKD) (1). The prevalence and risk of fractures are considerably increased in patients with CKD compared with healthy individuals (2). In particular, compared with the general population, patients on dialysis exhibit an approximately 4.4- to 14-fold increased risk of hip fractures (3,4). Cinacalcet (CINA), a calcimimetic agent that acts directly at the calcium-sensing receptor in the parathyroid gland to reduce parathyroid hormone (PTH) secretion, has been widely used for secondary hyperparathyroidism (SHPT) in patients with CKD (5). Recently evidence indicated that CINA therapy improved bone health by improving bone histology and reducing the incidence of fractures (6,7). However, the mechanism study of the skeletal effects about CINA is still unclear.

Traditionally, CKD-associated osteoporosis is usually caused by a variety of factors, including uremic toxins, vitamin D deficiency, electrolyte and acid-base disorders, medications, dialysis, anemia, inflammation and hypogonadism (8). Recently, the importance of bone marrow adipocytes (BMAs) in CKD-related bone loss has been increasingly appreciated (9). Anatomically, BMAs comprise approximately 70% of the bone marrow, accounting for 1.35 kg in weight or 8% of the total fat mass, with BMAs more predominantly observed in the appendicular skeleton than axial skeleton (10). Increased BMAs could decrease osteoblast differentiation and increase osteoclast formation (11,12). Adipocytes exerted a toxic effect on osteoblasts through the secretion of fatty acids, and inhibition of fatty acid synthase in ovariectomized mice could rescue fat-induced osteoblasts death and toxicity (13). These findings indicate that the accumulation of BMAs potentially underlies the progression of osteoporosis in subjects with CKD.

During the past decade, mesenchymal stem cells (MSCs) were considered the major precursors of BMAs (14) and contribute to subsequent bone loss. Recently, endothelial cells (ECs) were reported to participate in adipogenesis through a process known as the endothelial-to-mesenchymal transition (EndMT) (15,16). The EndMT is defined by the loss of cellular adhesion and cytoskeletal reorganization of actin and intermediate filaments that converts apical-basal polarity to front end-back end polarity and forms spindle-shaped cells (17). Numerous autocrine or paracrine signaling molecules produced by inflammation, tissue injury and cancer stimulate the EndMT (18). Transforming growth factor-β (TGF-β) and bone morphogenetic protein (BMP) are the most common inducers of the EndMT (19). Medici *et al.* (15) treated ECs with TGF-β or BMP-4 and observed their growth in adipogenic culture medium for a week. The authors found that ECs that underwent the EndMT acquired an MSC phenotype and then differentiated into adipocytes. As shown in the study by Huang *et al.* (20), endocardial-derived cushion MSCs migrate into the myocardium and differentiate into adipocytes during cardiac development and regeneration. Tran *et al.* (21) showed an endothelial origin of adipocytes in adipose tissue expansion. However, the physiological signals that determine adipocyte and EC fates remain unclear. Overall, the conversion of ECs to adipocytes might represent a novel approach to treat bone loss in patients with CKD.

Elevation of serum PTH levels is common in patients with CKD and SHPT (22). Hyperphosphatemia, hypovitaminosis D and hypocalcemia occurred, and fibroblast growth factor 23 levels increased as renal function declined, which stimulated PTH synthesis and resulted in parathyroid hyperplasia (23). PTH plays very important role in bone and mineral metabolism. Continuous exposure to high levels of PTH is associated with an increased incidence of bone fractures, and removal of the parathyroid glands from patients with CKD and SHPT significantly decreased bone resorption (24). Elevated PTH levels increased the expression of monocyte chemoattractantprotein-1 and the receptor activator of nuclear factor-κB ligand/osteoprotegerin (RANKL/OPG) ratio, which regulated bone resorption (25). However, the underlying mechanism of PTH mediated skeletal abnormalities remains largely unclear. Our preliminary *in vivo* and *in vitro* experiments revealed that increased PTH levels could cause the EndMT and the acquisition of a multipotent stem cell-like phenotype in ECs (26,27). However, researchers have not clearly determined whether the PTH-induced EndMT subsequently leads to the production of adipocytes.

In this study, we assessed whether CINA could attenuate

bone loss via inhibiting endothelial-to-adipocyte transition in CKD rats, which might provide a new mechanism for treating bone loss in patients with CKD.

Methods

Animals

The Institutional Animal Care and Use Committee of Southeast University (Nanjing, China) authorized our study. Eight-week-old male Sprague Dawley rats (Animal Laboratory of Nantong University, China) were randomly assigned to three groups: control group (CTL), CKD group, and CINA treated CKD group (CKD + CINA). Ten animals were included in each group. Our rat models of CKD with SHPT were induced by diets containing 0.75% adenine and high phosphorus (1.5%), as previously described (28). CINA (Kirin Pharmaceutical Company, USA), a calcimimetic agent that has been widely used to reduce PTH secretion in patients with CKD, was orally administrated once daily (10 mg/kg) for 34 weeks (29). Blood samples were collected to assess biochemical parameters, and tibia and femur samples were used for histology.

Serum biochemistry

Blood urea nitrogen, serum creatinine, phosphate and total calcium levels were measured using a UV-5100 spectrophotometer and semiautomatic biochemical analyzer (ECA-2000A). Serum PTH concentrations were determined using an ELISA (MEIMIAN). The coefficient of variation was <10%. The interval between the test time and blood collection time was <1 week. Repeated freeze-thaw cycles were avoided.

Dual-energy X-ray absorptiometry (DEXA)

A bone mineral DEXA analyzer of (HOLOGIC QDR series, America) was used to determine the bone mineral density (BMD) of femurs and lumbar vertebrae in each group at the Southeast University-affiliated Zhongda Hospital before the animals were sacrificed.

Micro-computed tomography (micro-CT)

Using micro-CT (SkyScan 1176, Germany), the trabecular bone volume (BV/TV, %) and architecture (trabecular thickness, spacing, and number) were determined from trabecular bone isolated from the metaphysis of the distal femur and the fourth lumbar vertebral body (L4). In addition, the tests were performed before the animals were sacrificed. Cortical bone geometry (cortical thickness and area) was determined from the femoral midshaft. Here, an 18-μm resolution was chosen to scan all animals under minimal anesthesia to avoid artifacts due to animal movements. The resulting images were reconstructed using the SkyScan software NRecon. The data were analyzed using CtAnalyser (SkyScan software). Three-dimensional images were obtained using CtVox (SkyScan software). The micro-CT parameters were reported according to the international guidelines (30).

Bone mechanics

The material properties and structural mechanical properties of the fifth lumbar vertebra (L5) were obtained by performing a uniaxial compression testing (Instron 5943, America). Samples were loaded at a rate of 0.5 mm/min to construct a force-displacement curve, and structural mechanical properties were obtained from these curves as previously described (31).

H&E staining

For H&E staining, bone tissues were fixed with 10% neutral buffered formalin, decalcified in 10% (w/v) ethylenediamine tetraacetic acid (EDTA) and embedded in paraffin. Sections were stained with H&E after deparaffinization and rehydration. Stained sections were mounted and histopathological changes were observed by one experienced pathologist using light microscope (32). The number of BMAs (#/mm^2) was calculated using the Image-Pro Plus analysis software, n=3 for each group.

Oil red O staining

The femurs were collected, and fixed with 4% (w/v) paraformaldehyde, decalcified in 10% (w/v) EDTA, and then embedded. Sections were mounted on slides and stained with oil red O. Stained sections were mounted and observed for histopathological changes and adipocyte measurements were observed under a light microscope. The number of BMAs per high power field was calculated in three randomly selected areas of sections using the Image-Pro Plus image analysis software, n=3 for each group.

Oil red O staining in cells was performed as described

in a previous study (33). Briefly, samples were fixed with 4% paraformaldehyde for 20 minutes and then stained with oil red O for 10 minutes. The red-colored intracellular lipid vesicles stained with oil red O were observed under a microscope, and lipid accumulations were quantified by measuring the absorbance at 500 nm.

Immunofluorescence staining

Paraffin sections or cells were plated in confocal dishes were fixed with 4% paraformaldehyde for 20 minutes, permeabilized with 0.25% Triton X-100 for 15 minutes, and blocked with 10% BSA in phosphate-buffered saline (PBS) for 1 hour at room temperature. Samples were then immunostained with primary antibodies against CD31 (sc-376764 from Santa Cruz, 1:300 dilution; ab-28364 from Abcam, 1:300 dilution), FSP1 (ab-197896, Abcam, 1:250 dilution), α-SMA (ab-7817, Abcam, 1:250 dilution) or CD44 (ab-157107, Abcam, 1:250 dilution) at 4 ℃ overnight. After an incubation with the secondary antibodies for 1 hour in the dark at room temperature, images were captured using a laser scanning confocal microscope (FV1000, Olympus).

Cell culture

Primary human aortic ECs were purchased from ScienCell Research Laboratories (catalog number: 6100, USA) and cultured as previously described (34). All experiments were performed using cells at passages 3 to 5. Cells were cultured in the presence of PTH (P3796, Sigma, USA, 10^{-7} mol/L) for 48 hours to identify the effects of PTH on the phenotypic transition and differentiation capability of ECs that undergo the EndMT,. Then, the ECs culture medium was replaced with the MSC adipogenic differentiation medium (catalog number: 7541, ScienCell Research Laboratories, USA) containing MSC adipogenic differentiation supplement (catalog number: 7542, ScienCell Research Laboratories, USA) for 7 days.

Transmission electron microscopy (TEM)

TEM was performed using to a routine fixation and embedding procedure to examine the ultrastructural changes of ECs (34). Cells were fixed with 2.5% glutaraldehyde. Tissues were embedded in Durcupan resin after fixation and dehydration. Then, sections were cut on a microtome, placed on copper grids, stained with uranyl acetate and lead citrate, and finally examined using a TEM (JEM-1010, JEOL, Japan) at the Electron Microscopy Core Facility.

Western blot analysis

Protein levels were detected using western blot analyses as described in a previous study (35). Briefly, the bone tissues and ECs were completely homogenized in radio immunoprecipitation assay (RIPA) lysis buffer, ultrasonically lysed and centrifuged. Finally, we collected the supernatant and placed it in separate Eppendorf tubes. Equal amounts of protein obtained from each lysate were separated onBis-Tris gels and transferred to polyvinylidene fluoride (PVDF) membranes. PVDF membranes were incubated overnight with primary antibodies against CD31 (sc-376764, Santa Cruz, 1:1,000 dilution), FSP1 (ab-197896, Abcam, dilution), α-SMA (ab-7817, Abcam, 1:1,000 dilution), CD10 (NBP2-15771, Novus Biologicals, 1:1,000 dilution), CD44 (ab-157107, Abcam, 1:1,000 dilution), C/EBP-α (sc-365318, Santa Cruz, 1:1,000 dilution), or PPAR-γ (ab-209350, Abcam, 1:1,000 dilution) followed by horseradish peroxidase-labeled secondary IgG (Santa Cruz). Signals were detected using an advanced ECL system (GE Healthcare). GAPDH (GB12002, Servicebio, 1:300 dilution) was used as internal standard. Finally, the immunoreactive bands were determined using densitometry with Image J software (NIH, Bethesda, USA).

Cell viability assay

Cell proliferation was determined using the CCK8 assay. Cells in the logarithmic phase growing in 96-well plates were analyzed. Each sample was plated on three plates, with three replicates per plate. The plates were cultured with 0, 10^{-11}, 10^{-9}, 10^{-7} mol/L PTH for 48 hours at 37 ℃ in a 5% CO_2 incubator. Then, the cells were incubated with 10 μL of CCK8 solution for 2 hours. The absorbance of each well was measured using a microplate reader (Multiskan GO 1510, Thermo Fisher) at 450 nm.

Statistical analyses

The data are presented as the mean ± standard deviation (SD) and were analyzed using one-way analysis of the variance (ANOVA) with SPSS version 21.0. The data were considered significant when $P<0.05$.

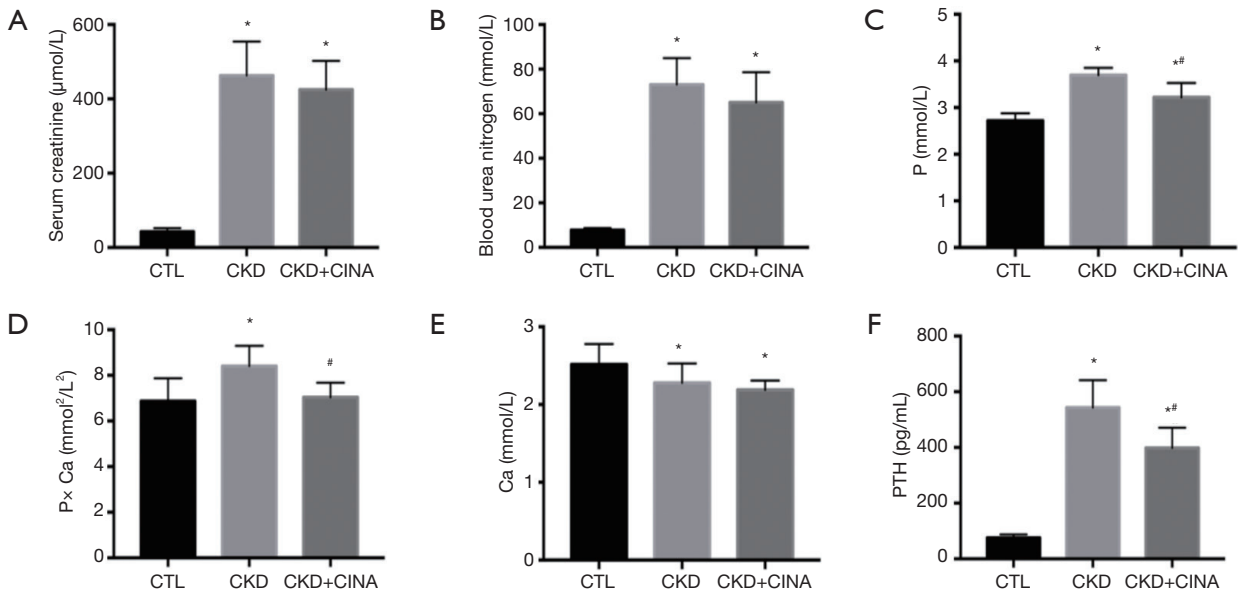

Figure 1 Analysis of (A) serum creatinine, (B) blood urea nitrogen, (C) P, (D) P× Ca product, (E) Ca and (F) PTH levels in the study groups. The data are expressed as the mean ± SD. n=10 for each group. *, P<0.05 *vs.* the CTL group; #, P<0.05 *vs.* the CKD group. CTL, control; CKD, chronic kidney disease; CINA, cinacalcet; PTH, parathyroid hormone; SD, standard deviation.

Results

Blood biochemical parameters of animals

As shown in *Figure 1*, animals with CKD had higher serum levels of creatinine (462.82±91.29 μmol/L) and blood urea nitrogen levels (73.08±11.87 mmol/L) than the control animals (serum creatinine, 42.75±9.48 μmol/L; blood urea nitrogen, 7.78±0.94 mmol/L), indicating the presence of renal dysfunction; serum levels of PTH (542.94± 98.51 pg/mL), phosphorus (3.69±0.16 mmol/L) andcalcium × phosphorus product (8.40±0.90 $mmol^2/L^2$) were all significantly higher in the rats with CKD than in their normal counterparts (CTL group: PTH75.90±12.10 pg/mL; phosphorus 2.72±0.16 mmol/L; calcium × phosphorus product6.87±1.00 $mmol^2/L^2$), while calcium levels decreased (2.28±0.25 *vs.* 2.52±0.26 mmol/L). CINA, a calcimimetic agent that is widely used to reduce PTH secretion, was administered to the CKD rats. CINA-treated animals presented lower levels of PTH (398.15±72.92 pg/mL), phosphorus (3.22±0.31 mmol/L), and calcium × phosphorus product (7.03±0.64 $mmol^2/L^2$) than their untreated CKD counterparts, although no significant changes in serum creatinine, blood urea nitrogen and calcium levels were observed.

CINA treatment attenuated bone loss in rats with CKD

Next, we study the effects of CINA on skeleton in CKD rats. The skeletal system was investigated using DEXA scanning, micro-CT analysis, bone mechanical analysis and bone histology (H&E staining).

As shown in *Figure 2A*, BMD, as determined using DEXA scanning, was significantly decreased in the CKD group compared to the CTL group (femur 0.22±0.02 *vs.* 0.26±0.02 g/cm^2; vertebra: 0.29±0.03 *vs.* 0.36±0.04 g/cm^2), and the change was alleviated by treatment with CINA (CKD+CINA group: femur 0.24±0.02 g/cm^2; vertebra 0.33±0.01 g/cm^2).

The femur and lumbar bone parameters measured using micro-CT are presented in *Table 1* and *Figure 2B*. In the distal femur, the BV/TV (29.39%±5.13%), trabecular thickness (Tb.Th, 0.10±0.01 mm), and trabecular number (Tb.N, 2.91±0.40 1/mm) were reduced, while trabecular separation (Tb.Sp, 0.18±0.02 mm) increased in the CKD group compared with the control group (CTL group: BV/TV 44.25%±1.00%; Tb.Th 0.12±0.02 mm; Tb.N 3.58± 0.73 1/mm; Tb.Sp 0.15±0.03 mm). The CINA treatment tended to increase the BV/TV (36.43%±2.71%) and Tb.N (3.53±0.29 1/mm) and decrease Tb.Sp (0.15±0.02 mm) in the CKD rats. In the femoral diaphysis, the cortical area

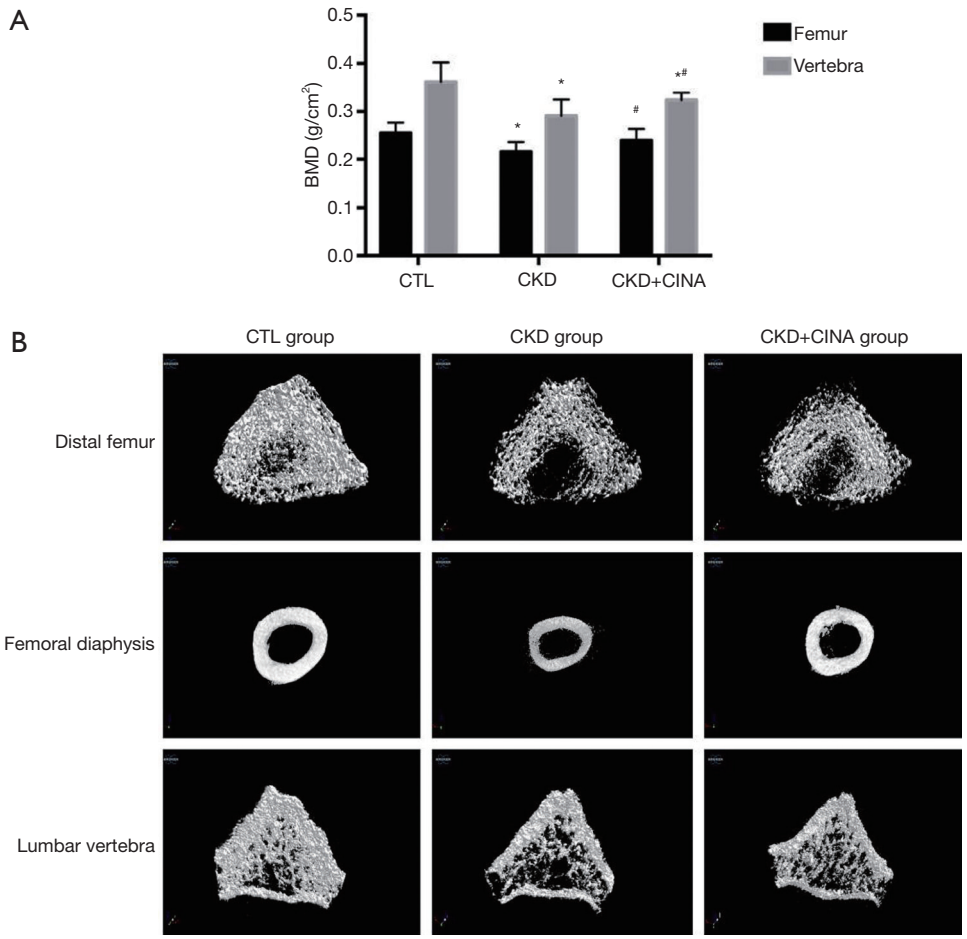

Figure 2 CINA treatment attenuates bone loss in the study group. (A) Analysis of the BMD of the left femur and lumbar vertebra in the study groups using dual-energy X-ray absorptiometry in the study group. The data are expressed as the mean ± SD. n=10 for each group. *, P<0.05 *vs.* the CTL group; #, P<0.05 *vs.* the CKD group. (B) Representative micro-computed tomography images of the distal femur, femoral diaphysis, and lumbar vertebra. The volume of the trabecular and cortical bone was significantly reduced in the CKD group, and the CINA treatment attenuated those changes. BMD, bone mineral density; CTL, control; CKD, chronic kidney disease; CINA, cinacalcet; SD, standard deviation.

(Ct.Ar, 4.64±1.57 mm^2) and cortical thickness (Ct.Th, 0.46±0.17 mm) were lower in the CKD group than in the control group (CTL group: Ct.Ar 6.34±1.46 mm^2; Ct.Th 0.65±0.14 mm), and the CINA treatment improved these parameters (Ct.Ar, 6.34±1.90 mm^2; Ct.Th, 0.61±0.19 mm). In the lumbar vertebra, the BV/TV (16.275%±2.21%), Tb.Th (0.053±0.005 mm) and Tb.N (3.00±0.29 1/mm) were reduced in the CKD group compared with the control group (CTL group: BV/TV 22.70%±2.43%, Tb.Th 0.059±0.002 mm and Tb.N 3.85±0.46 1/mm). Treatment with CINA tended to increase the BV/TV (18.466%±2.16%) and Tb.N (3.37±0.36 1/mm). In addition, a lower Ct.Th (0.10±0.01 mm) was observed in the CKD group than in the control group (Ct.Th 0.13±0.01 mm), and the CINA treatment did not change this parameter.

Vertebral compression test revealed that CKD rats exhibited reductions in the ultimate force (251.26±17.46 N), work to failure (52.47±10.98 mJ), stiffness (502.20± 102.75 N/mm) and elastic modulus (337.63±152.49 MPa) compared with the normal animals (CTL group: ultimate force 307.62±55.75 N, work to failure 112.40±31.82 mJ, stiffness 962.85±49.38 N/mm and elastic modulus 652.72±103.49 MPa). The CINA treatment increased stiffness (737.09±84.39 N/mm) when compared with that of

Table 1 Micro-CT

Parameter	CTL (n=10)	CKD (n=10)	CKD + CINA (n=10)
Distal femur			
BV/TV (%)	44.25±1.00	29.39±5.13*	36.43±2.71*#
Tb.Th (mm)	0.12±0.02	0.10±0.01*	0.10±0.01*
Tb.N (1/mm)	3.58±0.73	2.91±0.40*	3.53±0.29#
Tb.Sp (mm)	0.15±0.03	0.18±0.02*	0.15±0.02#
Femoral diaphysis			
Ct.Ar (mm^2)	6.34±1.46	4.64±1.57*	6.34±1.90#
Ct.Th (mm)	0.65±0.14	0.46±0.17*	0.61±0.19#
Lumbar vertebra			
BV/TV (%)	22.70±2.43	16.275±2.21*	18.466±2.16*#
Tb.Th (mm)	0.059±0.002	0.053±0.005*	0.055±0.004*
Tb.N (1/mm)	3.85±0.46	3.00±0.29*	3.37±0.36*#
Tb.Sp (mm)	0.14±0.02	0.15±00.02	0.15±0.02
Ct.Th (mm)	0.13±0.01	0.10±0.01*	0.10±0.02*

The results are presented as the means ± SD (n=10 for each group). *, P<0.05 *vs.* the CTL group; #, P<0.05 *vs.* the CKD group. BV/TV, bone volume fraction; Tb.Th, trabecular thickness; Tb.Sp, trabecular separation; Tb.N, trabecular number; Ct.Ar, cortical area; Ct.Th, cortical thickness; CTL, control; CKD, chronic kidney disease; CINA, cinacalcet.

Table 2 bone mechanics

Parameter	CTL (n=5)	CKD (n=5)	CKD + CINA (n=5)
Ultimate force (N)	307.62±55.75	251.26±17.46*	268.30±25.41*
Displacement (mm)	0.72±0.17	0.72±0.13	0.71±0.11
Work to failure (mJ)	112.40±31.82	52.47±10.98*	49.56±10.05*
Stiffness (N/mm)	962.85±49.38	502.20±102.75*	737.09±84.39*#
Maximum stress (MPa)	36.63±8.91	36.50±15.10	39.07±8.56
Maximum strain (MPa)	0.13±0.02	0.13±0.04	0.13±0.01
Toughness (MPa)	2.17±0.66	1.89±0.53	2.20±0.53
Elastic modulus (MPa)	652.72±103.49	337.63±152.49*	356.29±116.80*

The data are expressed as the means ± SD. n=5 for each group. *, P<0.05 *vs.* the CTL group; #, P<0.05 *vs.* the CKD group. CTL, control; CKD, chronic kidney disease; CINA, cinacalcet.

rats in the CKD group (*Table 2*).

Histopathological investigation of the rat tibia bone sections revealed a well-formed and connected bone with normal thickness and density in rats in the CTL group. Tibia bones from the CKD group exhibited widely separated and uniform thinning of the trabeculae, resulting in osteoporosis. The CINA treatment resulted in a slight thinning of bone trabeculae, improving osteoporosis in CKD rats (*Figure 3A*).

CINA treatment decreased the number of BMAs in rats with CKD

We further detected BMA infiltration in the study groups.

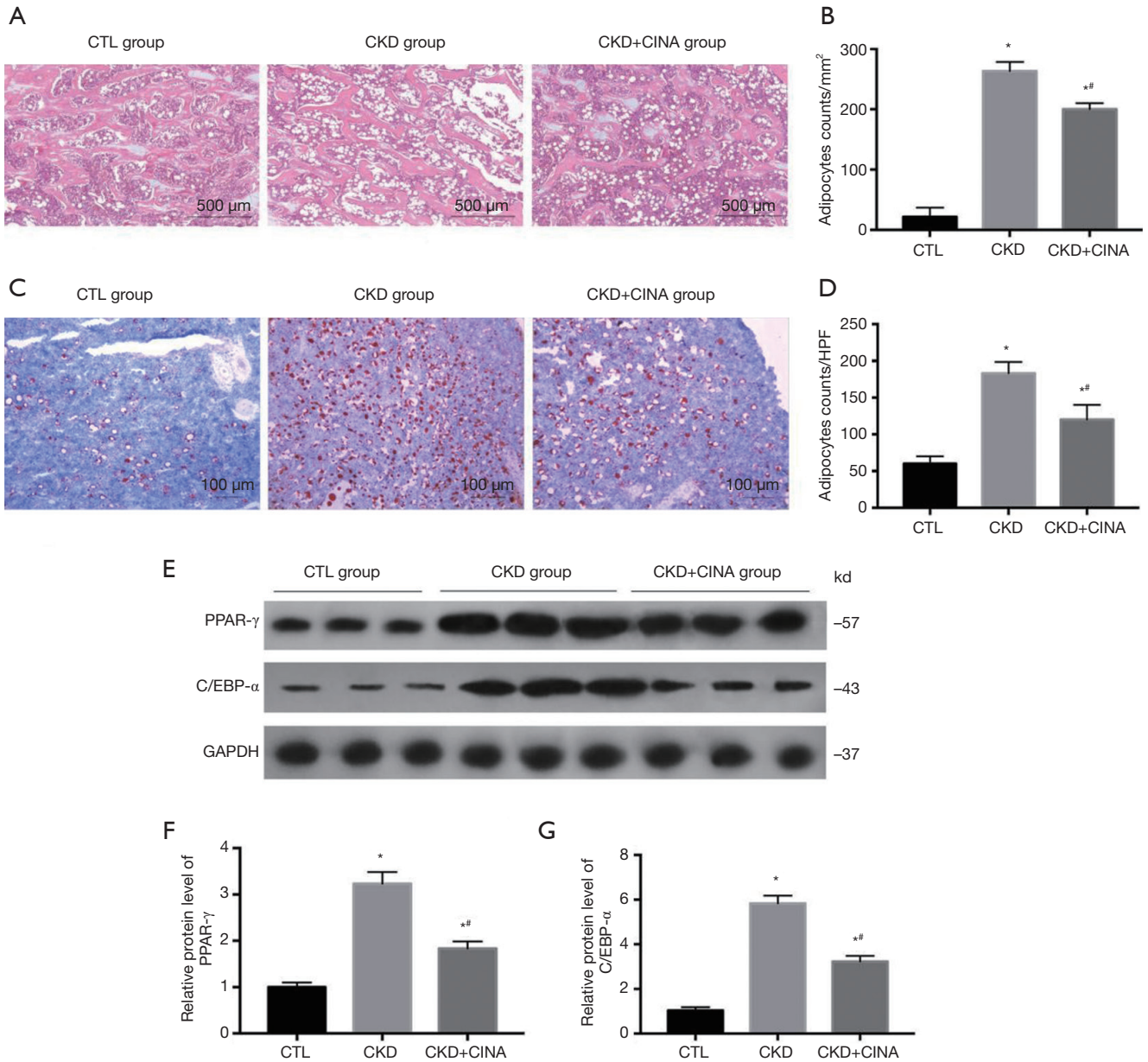

Figure 3 CINA treatment decreases BMAs in CKD rats. (A) Images of H&E staining in the tibia sections from the study groups. Scale bar, 500 μm; (B) adipocyte counts per mm^2 in tibial bone marrow sections; (C) oil red O staining of the femur in the study group. Scale bar, 100 μm; (D) adipocyte counts per HPF in femoral bone marrow sections; (E) western blot analysis showing the levels of adipocyte markers proteins (PPAR-γ, C/EBP-α) in the different groups of rats, as indicated; (F,G) statistical analysis of the western blot results for the levels of the PPAR-γ and C/EBP-α proteins. The data are presented as the mean ± SD. n=3 for each group. *, P<0.05 *vs.* the CTL group; #, P<0.05 *vs.* the CKD group. HPF, high-power field; CTL, control; CKD, chronic kidney disease; CINA, cinacalcet; BMA, bone marrow adipocyte; SD, standard deviation.

Adipogenesis was increased in CKD compared with the controls. This change was reversed by the CINA treatment (*Figure 3A,B,C,D*). In addition, the bone marrow protein levels of adipocyte markers proteins (PPAR-γ and C/EBP-α) were increased in CKD animals, and these values were reduced by the CINA treatment (*Figure 3E,F,G*).

CINA treatment inhibited bone marrow EndMT in rats with CKD

As determined by using western blot analyses (*Figure 4A,B*), levels of the endothelial marker CD31 was significantly decreased in bone marrow of CKD rats, whereas the expression levels of mesenchymal markers (FSP1 and α-SMA) and MSC markers (CD10 and CD44) were markedly increased. These changes were inhibited by the CINA treatment. In addition, confocal microscopy revealed an increased colocalization of CD31 and FSP1, as well as CD31 and CD44, in bone marrow from the CKD group compared with controls (*Figure 4C*, white arrows). The administration of CINA abrogated these changes.

Serum PTH levels correlated with EndMT marker expression

As shown in *Figure 5*, a significant negative correlation was observed between serum PTH levels and bone marrow levels of the CD31 protein levels ($r=-0.87$, $P<0.01$) in different group. In addition, FSP1 and α-SMA expression positively correlated with serum PTH levels ($r=0.85$, $P<0.01$, for FSP1; $r=0.82$, $P<0.01$, for α-SMA). The results from these *in vivo* studies indicated an important role for serum PTH levels in the bone marrow EndMT.

PTH triggered the EndMT in cultured ECs

We performed *in vitro* experiments using cultured primary human aortic ECs, which have been extensively characterized as a population of homogeneous ECs in previous studies, to further confirm the effects of PTH on bone marrow EndMT. We treated ECs with PTH at concentrations ranging from 0 to 10^{-7} mol/L. ECs exposed to 10^{-7} mol/L PTH acquired a spindle-shaped morphology resembling the phenotypic changes typically associated with the EndMT (*Figure 6A*). In addition, the cytotoxic effect of PTH on cell viability was evaluated by CCK8 test at various concentration (0, 10^{-11}, 10^{-9}, 10^{-7} mol/L) for 48 hours. The results revealed that PTH stimulation did not alter cell viability compared to controls (*Figure 6B*). This result indicated that PTH concentration in the range of 10^{-11}, –10^{-7} mol/L showed no cytotoxicity on ECs. Consistent with the findings described above, an electron microscopy analysis of the CTL group revealed normal structures of the ECs. In contrast, the PTH (10^{-7} mol/L) group exhibited considerable microfilamentation (*Figure 6C*, red arrow), which is typical of fibroblasts.

We performed immunofluorescence double-labeling experiments using antibodies specific for CD31 and α-SMA to corroborate these observations (*Figure 6D,E*). The acquisition of the spindle-shaped morphology in response to PTH was associated with the loss of the endothelial marker CD31 and *de novo* expression of the myofibroblast marker α-SMA, which is a characteristic of the EndMT. Accordingly, PTH induced the EndMT in a concentration- and time-dependent manner (*Figure 6F,G,H,I*). The aforementioned results confirmed that PTH triggered the EndMT in ECs, and that ECs incubated with PTH (10^{-7} mol/L) for 48 hours exhibited the most remarkable phenotypic changes.

The EndMT induced the adipogenic potential of ECs

We next assessed the differentiation capability of ECs that underwent the EndMT. Based on the results described above, we treated ECs with 10^{-7} mol/L PTH for 48 hours and then changed the ECs culture medium to an adipogenic culture medium for 7 days. Western blot analyses indicated significantly increased levels of adipocyte markers (PPAR-γ and C/EBP-α) in ECs cultured with PTH followed by exposure to adipogenic culture medium compared with the CTL group (*Figure 7A,B*). In addition, the oil red O staining showed positive staining for adipocytes in the ECs of the PTH group (*Figure 7C,D*). Thus, the cells that undergo the EndMT further differentiated into adipocytes, confirming that elevated PTH levels induced the endothelial-to-adipocyte transition.

Discussion

Patients with CKD have an increased risk of osteoporosis, potentially due to the increased infiltration of BMAs (9,36). CINA have been reported to reduce serum PTH levels in patients with CKD, but the skeletal effects have not been adequately characterized. Our study showed that CINA treatment significantly attenuated bone loss and decreased BMAs in CKD rats. The beneficial effects on skeleton might be that CINA decreased BMAs by inhibiting the PTH-induced endothelial-to-adipocyte transition.

SHPT is a common complication in patients with CKD. Elevation of serum PTH levels due to SHPT exacerbates an imbalance in minerals and bone disorders in CKD (37,38), which leads to severe bone disorders in CKD (39).

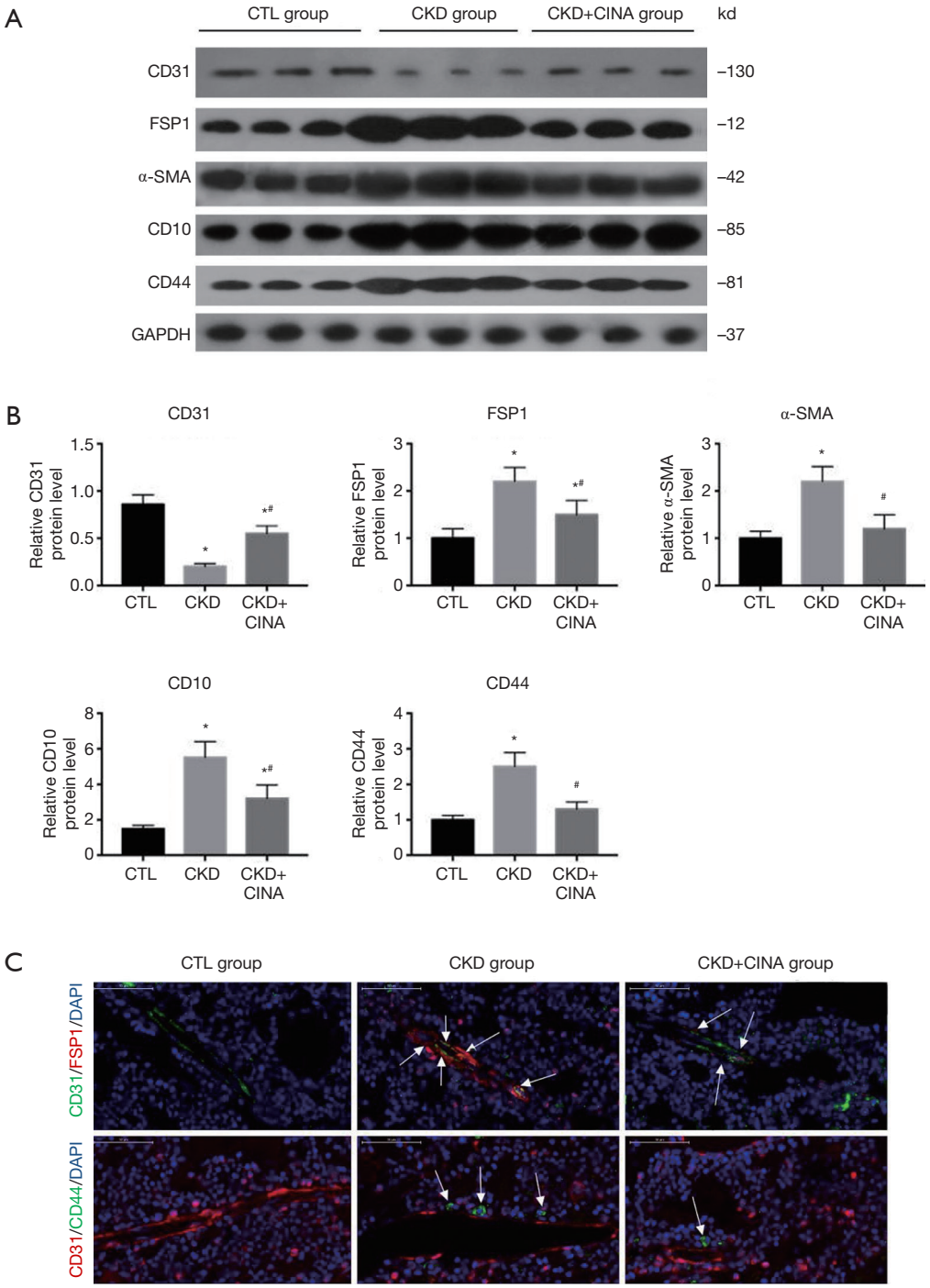

Figure 4 CINA treatment inhibits the EndMT in CKD rats. (A,B) Representative western blot analysis and quantification of levels of the CD31, FSP1, α-SMA, CD10, and CD44 proteins in the different groups of rats, as indicated. The data are presented as the mean ± SD. n=4 for each group. *, P<0.05 *vs.* the CTL group; #, P<0.05 *vs.* the CKD group. (C) Representative images of immunofluorescence staining for CD31, FSP1, and CD44 in the bone marrow of rats (upper panel: green for CD31, red for FSP1; lower panel: red for CD31, green for CD44). White arrows indicate colocalization between CD31 and either FSP1 or CD44. DAPI (blue) labels the nuclei. Scale bar, 50 μm. CTL, control; CKD, chronic kidney disease; CINA, cinacalcet; SD, standard deviation.

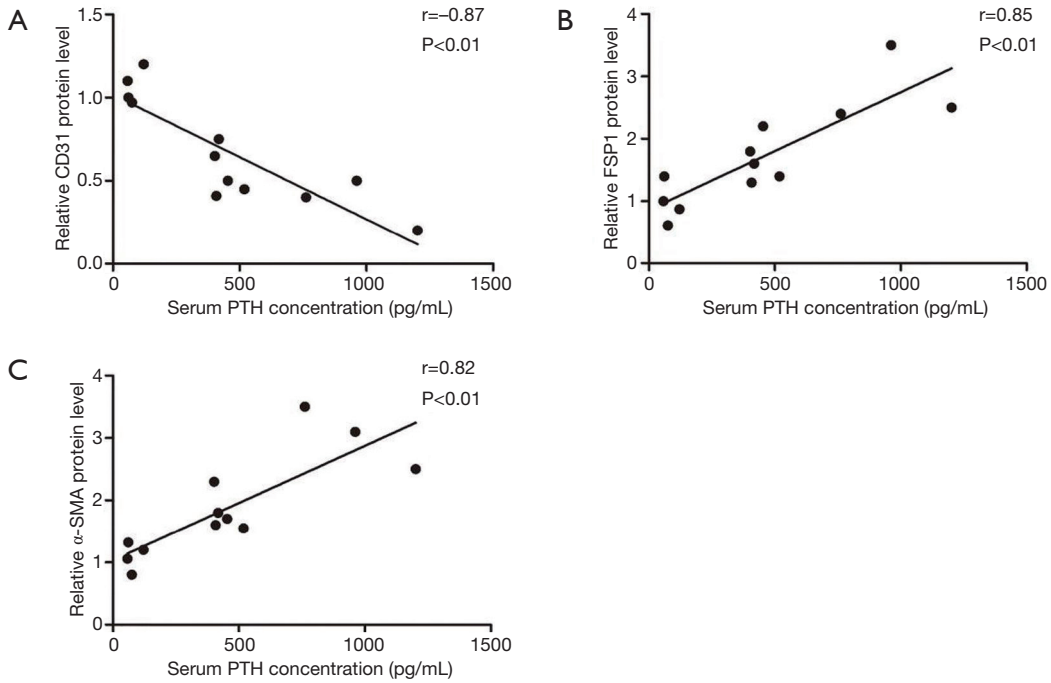

Figure 5 Relationship between the serum PTH concentration and protein levels of the CD31 (A), FSP1 (B) and α-SMA (C) proteins in in different group (n=4 rats/group). PTH, parathyroid hormone.

In our study, a rat model of CKD and SHPT was induced by adenine and a high phosphorus diet, as previously described (28). An analysis of the animals' skeletal structures was performed using multiple methods (e.g., DEXA scanning, micro-CT analysis, and bone mechanical tests). An apparent decrease in BMD (femur: –16%; lumbar vertebra: –20%) was observed in CKD rats using DEXA scanning (*Figure 2A*). A micro-CT analysis, which is a more precise metric, further confirmed trabecular and cortical bone loss in CKD animals (*Table 1* and *Figure 2B*). In addition, the CKD animals exhibited compromised mechanical properties (*Table 2*), which might be attributed to the reduced cortical and trabecular bone mass. Based on these results, CKD animals presented severe bone loss. CINA treatment significantly decreased serum PTH levels and improved these skeletal abnormalities. The beneficial skeletal effects of CINA are consistent with several early studies in uremic animal models (40), renal transplant patients with SHPT (41), and hemodialysis patients (42). These bone-friendly effects may have been attributable to the reduction in serum PTH levels (43). However, the exact mechanism for CINA on skeletal disease in rats with CKD remains largely unclear.

Recently, the importance of BMAs in the skeleton has been increasingly appreciated. Three possible mechanisms could explain how adiposity influences skeletal abnormalities (44): First, endocrine cytokines and growth factors released by adipocytes affect osteoblasts and osteoclasts. Second, adipokines (e.g., leptin and adiponectin) regulate the central nervous system via the sympathetic nervous system. Third, paracrine factors secreted by adipocytes within the bone marrow milieu influence nearby cells on trabecular bone surfaces. In addition, strategies targeting BMAs have been shown to promote bone regeneration (10,45). Patients with CKD have significantly more BMAs than healthy adults (9,36). Consistent with these findings, our study revealed more BMAs in CKD rats compared with the normal controls, and the increase was attenuated by the CINA treatment (*Figure 3*). Considering the adverse effects of BMAs, it's possible that CINA treatment could alleviate osteoporosis by decreasing BMAs.

What is the mechanism underlying this process? Traditionally, bone marrow-derived MSCs have been the best characterized source of adipocyte progenitors for adipogenesis (46). Recently, cells of endothelial origin have also been shown to promote adipogenesis (15,47). Under certain conditions, vascular ECs undergo the EndMT, transform into MSCs, and subsequently differentiate

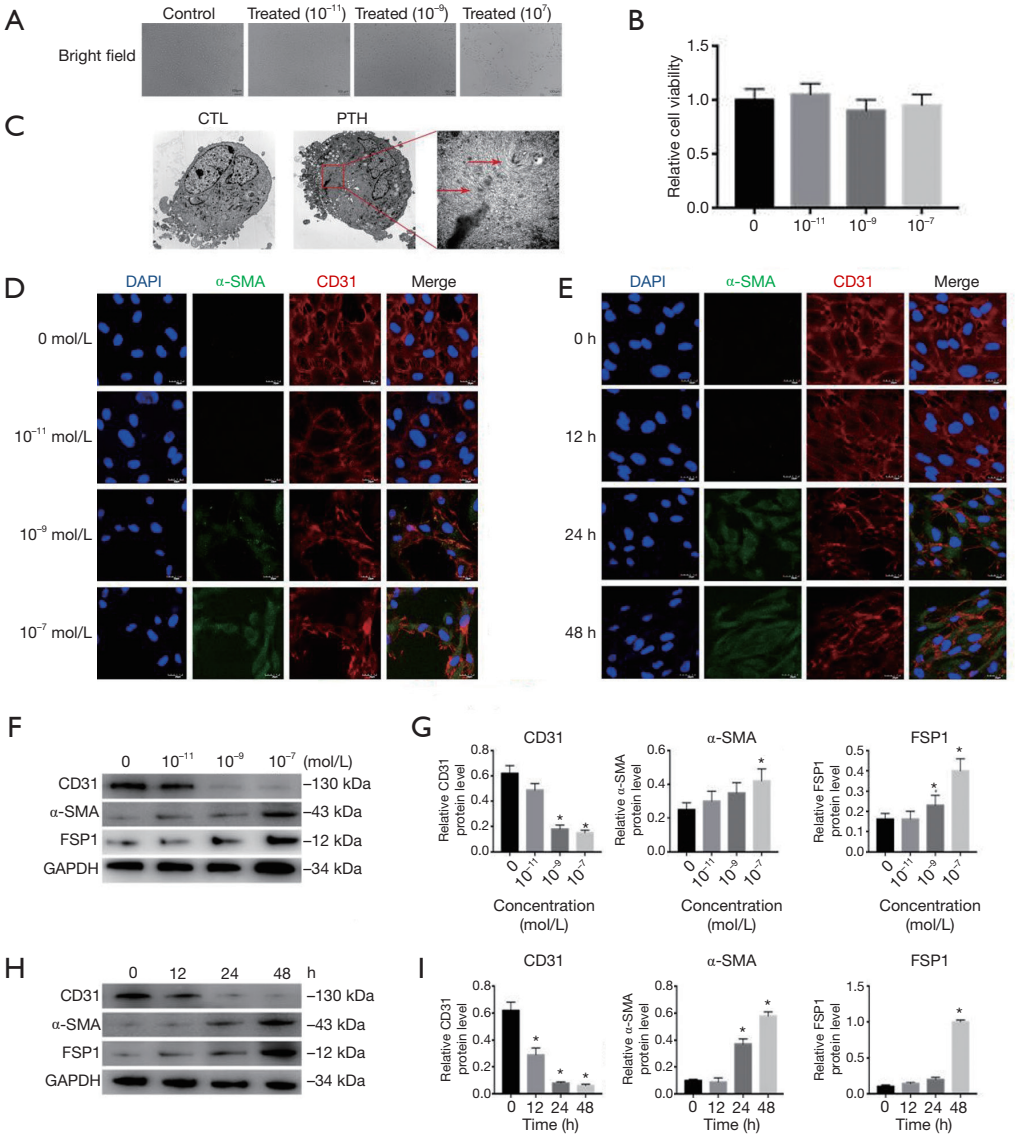

Figure 6 PTH triggers the EndMT in cultured ECs. (A) Bright field images showing the morphological changes in ECs that had been incubated with PTH (0, 10^{-11}, 10^{-9}, or 10^{-7} mol/L) for 48 hours compared with control cells. Compared with control cells, ECs lost their cobblestone appearance. Scale bars, 100 μm. (B) Effects of PTH on cell cytotoxicity in ECs. Cells were cultured with PTH for 48 hours. Cell viability was measured by CCK-8 test. The data are presented as the mean ± SD. All experiments were repeated for three times. (C) Transmission electronic microscopy images depict the changes in the ultrastructure of ECs. After exposure to PTH, microfilamentation appeared in the cytoplasm (left two panels: 10,000× magnification, right panel: 40,000× magnification). (D) Representative images of immunofluorescence staining for CD31 (red) and α-SMA (green) staining in ECs treated with various concentrations of PTH (0, 10^{-11}, 10^{-9}, or 10^{-7} mol/L) for 48 hours; the nuclei were counterstained with DAPI (blue). Scale bars, 20 μm. (E) Representative images of immunofluorescence staining for CD31 (red) and α-SMA (green) staining after exposure to 10^{-7} mol/L PTH for different periods of time (0, 12, 24, or 48 hours). The nuclei were counterstained with DAPI (blue). Scale bars, 20 μm. (F,G) ECs were incubated with increasing concentrations of PTH, as indicated, for 48 hours. Protein expression levels were determined using western blotting. The data are presented as the mean ± SD. n=3 samples per group. *, P<0.05 *vs.* 0 group. (H,I) ECs were incubated with PTH (10^{-7} mol/L) for different time periods, as indicated. Protein expression levels were determined using western blotting. The data are presented as the mean ± SD. n=3 samples per group. *, P<0.05 *vs.* 0 group. PTH, parathyroid hormone; ECs, endothelial cells; EndMT, endothelial-to-adipocyte transition; SD, standard deviation.

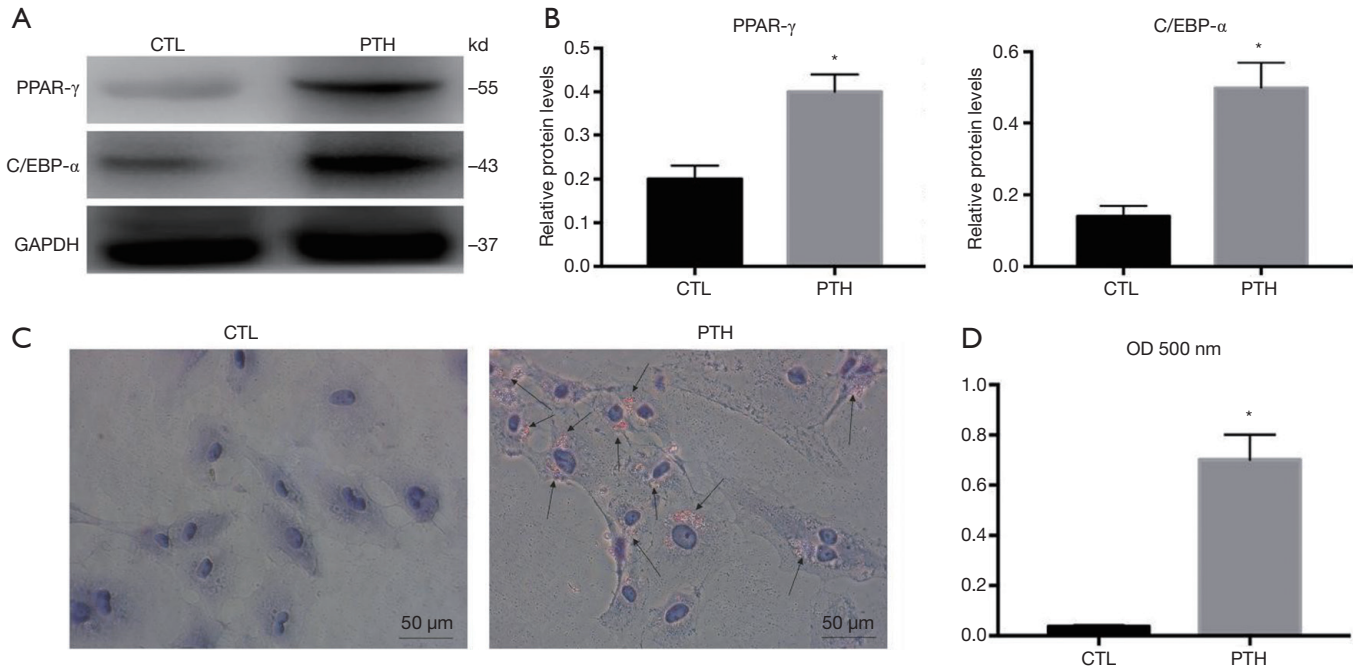

Figure 7 ECs that undergo the PTH-induced EndMT exhibit adipogenic potential. (A,B) Representative western blot analysis and quantification of PPAR-γ and C/EBP-α (adipocyte-specific markers) levels in cells treated with PTH (10^{-7} mol/L) for 48 hours followed by growth in adipogenic culture medium for 7 days. The data are presented as the mean ± SD. n=3 samples per group. *, P<0.05 *vs.* the CTL group. (C,D) Oil red O staining and quantification in EC cultures treated with PTH for 48 hours followed by growth in adipogenic culture medium (original magnification, 400×). The data are presented as the mean ± SD. n=3 samples per group. *, P<0.05 *vs.* the CTL group. PTH, parathyroid hormone; EC, endothelial cell; EndMT, endothelial to adipocyte transition; SD, standard deviation.

into adipocytes, osteoblasts and chondrocytes. Medici *et al.* (15) treated ECs with TGF-β or BMP-4, followed by growth in adipogenic culture medium for a week. The authors found that ECs that undergo the EndMT acquire an MSC phenotype and then differentiate into adipocytes. According to Lin *et al.* (48), tumor-induced bone formation is partially derived from tumor-associated ECs that have undergone the endothelial-to-osteoblast conversion, leading to the osteoblastic bone metastasis of prostate cancer. As shown in our previous studies (26,27,49), increased PTH levels induces the phenotypic transition of ECs to chondrocytes via the EndMT, and this conversion is involved in vascular calcification. In our *in vivo* experiment presented here, CINA treatment attenuated bone marrow EndMT in CKD animals (*Figure 4*). Moreover, serum PTH levels correlated with the levels of EndMT-related proteins in bone marrow (*Figure 5*). The *in vitro* experiment also showed that elevated PTH levels induced the phenotypic transition of ECs to adipocytes via the EndMT (*Figures 6* and 7). Based on these findings, we assumed that the beneficial skeletal effects of CINA treatment might be related with the inhibition of PTH-induced bone marrow endothelial-to-adipocyte transition, although the exact mechanism still needs to investigate.

Interesting, our study suggested that elevated PTH levels increased adipogenesis via the EndMT in ECs. However, there is evidence that PTH elicits a bone anabolic effect by inhibiting adipogenesis: intermittent exposure of human bone marrow-derived MSCs to teriparatide reduces adipocyte differentiation (50); Pth1r ablation in mesenchymal progenitors results in a decrease in bone mass and an increase in the number of BMAs in mice (51). In our study, high level of PTH increased the adipogenesis via EndMT in ECs. A potential explanation for these discrepancies is that the final effect on adipogenesis appears to depend on the duration and periodicity of PTH exposure and the target cell lineages. Our study could be an important complement to the existing research on the dual role of PTH in adipogenesis.

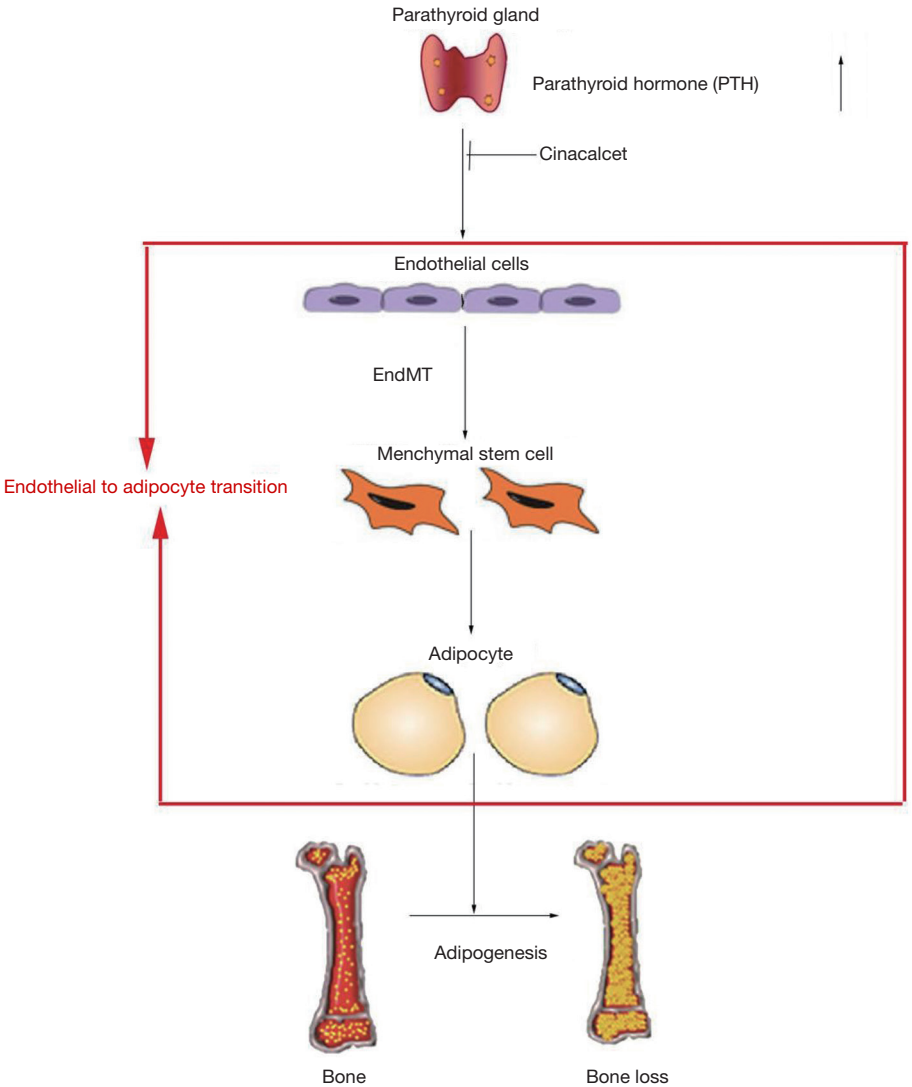

Figure 8 Schematic diagram of this study. Cinacalcet attenuates bone loss through inhibiting bone marrow endothelial-to-adipocyte transition via EndMT. EndMT, endothelial-to-mesenchymal transition.

Actually, CKD related osteoporosis is poorly understood and many factors in addition to PTH are involved in skeletal abnormalities in patients with CKD. Our study indicated a potential effect of PTH on BMAs, which might be an additional component of the complex situation of renal osteodystrophy.

In summary, our study showed that CINA treatment attenuated bone loss in CKD rats, which might be associated with the inhibition of PTH-induced bone marrow endothelial-to-adipocyte transition (*Figure 8*). These findings warrant translational investigations regarding of PTH suppression as the treatment for the skeletal disorders observed in subjects with CKD.

Acknowledgments

Funding: This study was funded by grants from the National Natural Science Foundation of China (31571186, 81770735, 81370919, 81470997), The Medical Talents of Jiangsu Province (ZDRCA2016079), the Natural Science Foundation of Jiangsu Province (BK20161437), Clinical Medicine Science and Technology Project-Clinic Research Center of Jiangsu Province (BL2014080), and Jiangsu Commission of Health "Six One Project" (LGY2018097).

Footnote

Conflicts of Interest: The authors have no conflicts of interest to declare.

Ethical Statement: The Institutional Animal Care and Use Committee of Southeast University (Nanjing, China) authorized our study. The authors are accountable for all aspects of the work (if applied, including full data access, integrity of the data and the accuracy of the data analysis) in ensuring that questions related to the accuracy or integrity of any part of the work are appropriately investigated and resolved.

References

1. Fusaro M, Aghi A, Mereu MC, et al. Fragility fracture in the Chronic Kidney Disease (CKD). G Ital Nefrol 2017;34.
2. Nickolas TL, McMahon DJ, Shane E. Relationship between moderate to severe kidney disease and hip fracture in the United States. J Am Soc Nephrol 2006;17:3223-32.
3. Coco M, Rush H. Increased incidence of hip fractures in dialysis patients with low serum parathyroid hormone. Am J Kidney Dis 2000;36:1115-21.
4. Mittalhenkle A, Gillen DL, Stehman-Breen CO. Increased risk of mortality associated with hip fracture in the dialysis population. Am J Kidney Dis 2004;44:672-9.
5. Wang G, Liu H, Wang C, et al. Cinacalcet versus Placebo for secondary hyperparathyroidism in chronic kidney disease patients: a meta-analysis of randomized controlled trials and trial sequential analysis. Sci Rep 2018;8:3111.
6. Behets GJ, Spasovski G, Sterling LR, et al. Bone histomorphometry before and after long-term treatment with cinacalcet in dialysis patients with secondary hyperparathyroidism. Kidney Int 2015;87:846-56.
7. Moe SM, Abdalla S, Chertow GM, et al. Effects of Cinacalcet on Fracture Events in Patients Receiving Hemodialysis: The EVOLVE Trial. J Am Soc Nephrol 2015;26:1466-75.
8. Zheng CM, Zheng JQ, Wu CC, et al. Bone loss in chronic kidney disease: Quantity or quality? Bone 2016;87:57-70.
9. Woods GN, Ewing SK, Sigurdsson S, et al. Chronic kidney disease is associated with greater bone marrow adiposity. J Bone Miner Res 2018;33:2158-64.
10. Scheller EL, Cawthorn WP, Burr AA, et al. Marrow adipose tissue: trimming the fat. Trends Endocrinol Metab 2016;27:392-403.
11. Hardouin P, Pansini V, Cortet B. Bone marrow fat. Joint Bone Spine 2014;81:313-9.
12. Hardouin P, Rharass T, Lucas S. Bone marrow adipose tissue: To be or not to be a typical adipose tissue? Front Endocrinol (Lausanne) 2016;7:85.
13. Bermeo S, Al Saedi A, Vidal C, et al. Treatment with an inhibitor of fatty acid synthase attenuates bone loss in ovariectomized mice. Bone 2019;122:114-22.
14. Bruedigam C, Eijken M, Koedam M, et al. A new concept underlying stem cell lineage skewing that explains the detrimental effects of thiazolidinediones on bone. Stem Cells 2010;28:916-27.
15. Medici D, Shore EM, Lounev VY, et al. Conversion of vascular endothelial cells into multipotent stem-like cells. Nat Med 2010;16:1400-6.
16. Medici D. Endothelial-Mesenchymal Transition in Regenerative Medicine. Stem Cells Int 2016;2016:6962801.
17. Hong L, Du X, Li W, et al. EndMT: A promising and controversial field. Eur J Cell Biol 2018;97:493-500.
18. Piera-Velazquez S, Jimenez SA. Endothelial to Mesenchymal Transition: Role in Physiology and in the Pathogenesis of Human Diseases. Physiol Rev 2019;99:1281-324.
19. Zeisberg EM, Tarnavski O, Zeisberg M, et al. Endothelial-to-mesenchymal transition contributes to cardiac fibrosis. Nat Med 2007;13:952-61.
20. Huang X, Feng T, Jiang Z, et al. Dual lineage tracing identifies intermediate mesenchymal stage for endocardial contribution to fibroblasts, coronary mural cells and adipocytes. J Biol Chem 2019;294:8894-906.
21. Tran KV, Gealekman O, Frontini A, et al. The vascular endothelium of the adipose tissue gives rise to both white and brown fat cells. Cell Metab 2012;15:222-9.
22. Evenepoel P, Bover J, Pablo Ureña P. Parathyroid hormone metabolism and signaling in health and chronic kidney disease. Kidney Int 2016;90:1184-90.
23. Saliba W, EI-Haddad B. Secondary hyperparathyroidism: pathophysiology and treatment. J Am Board Fam Med 2009;22:574-81.
24. Peters BS, Moyses RM, Jorgetti V, et al. Effects of parathyroidectomy on bone remodeling markers and vitamin D status in patients with chronic kidney disease-mineral and bone disorder. Int Urol Nephrol 2007;39:1251-6.
25. Qin L, Raggatt LJ, Partridge NC. Parathyroid hormone: a double-edged sword for bone metabolism. Trends Endocrinol Metab 2004;15:60-5.
26. Wu M, Tang RN, Liu H, et al. Cinacalcet ameliorates aortic calcification in uremic rats via suppression of endothelial-to-mesenchymal transition. Acta Pharmacol Sin 2016;37:1423-31.

27. Wu M, Tang RN, Liu H, et al. Cinacalcet ameliorates cardiac fibrosis in uremic hearts through suppression of endothelial-to-mesenchymal transition. Int J Cardiol 2014;171:e65-9.
28. Ni LH, Tang RN, Lv LL, et al. A rat model of SHPT with bone abnormalities in CKD induced by adenine and a high phosphorus diet. Biochem Biophys Res Commun 2018;498:654-9.
29. Henley C, Colloton M, Cattley RC, et al. 1,25-Dihydroxyvitamin D3 but not cinacalcetHCl (Sensipar/Mimpara) treatment mediates aortic calcification in a rat model of secondary hyperparathyroidism. Nephrol Dial Transplant 2005;20:1370-7.
30. Bouxsein ML, Boyd SK, Christiansen BA, et al. Guidelines for assessment of bone microstructure in rodents using micro-computed tomography. J Bone Miner Res 2010;25:1468-6.
31. Campbell GM, Tiwari S, Hofbauer C, et al. Effects of parathyroid hormone on cortical porosity, non-enzymatic glycation and bone tissue mechanics in rats with type 2 diabetes mellitus. Bone 2016;82:116-21.
32. Wang W, Zhang Y, Lu W, et al. Mitochondrial reactive oxygen species regulate adipocyte differentiation of mesenchymal stem cells in hematopoietic stress induced by arabinosylcytosine. PLoS One 2015;10:e0120629.
33. Ma KL, Ruan XZ, Powis SH, et al. Inflammatory stress exacerbates lipid accumulation in hepatic cells and fatty livers of apolipoprotein E knockout mice. Hepatology 2008;48:770-81.
34. Zhu DD, Tang RN, Lv LL, et al. Interleukin-1beta mediates high glucose induced phenotypic transition in human aortic endothelial cells. Cardiovasc Diabetol 2016;15:42.
35. Leiblein M, Henrich D, Fervers F, et al. Do antiosteoporotic drugs improve bone regeneration in vivo? Eur J Trauma Emerg Surg 2019. [Epub ahead of print].
36. Moorthi RN, Fadel W, Eckert GJ, et al. Bone marrow fat is increased in chronic kidney disease by magnetic resonance spectroscopy. Osteoporos Int 2015;26:1801-7.
37. Drüeke TB. The pathogenesis of parathyroid gland hyperplasia in chronic renal failure. Kidney Int 1995;48:259-72.
38. Fraser WD. Hyperparathyroidism. Lancet 2009;374:145-58.
39. Chen H, Han X, Cui Y, et al. Parathyroid Hormone Fragments: New Targets for the Diagnosis and Treatment of Chronic Kidney Disease-Mineral and Bone Disorder. Biomed Res Int 2018;2018:9619253.
40. De Schutter TM, Behets GJ, Jung S, et al. Restoration of bone mineralization by cinacalcet is associated with a significant reduction in calcitriol-induced vascular calcification in uremic rats. Calcif Tissue Int 2012;91:307-15.
41. Bergua C, Torregrosa JV, Fuster D, et al. Effect of cinacalcet on hypercalcemia and bone mineral density in renal transplanted patients with secondary hyperparathyroidism. Transplantation 2008;86:413-7.
42. Toro Prieto FJ, Bernal Blanco G, Navarro García M, et al. Calcimimetics and bone mineral density in renal transplant patients with persistent secondary hyperparathyroidism. Transplant Proc 2009;41:2144-7.
43. Foldes AJ, Arnon E, Popovtzer MM. Reduced speed of sound in tibial bone of haemodialysed patients: association with serum PTH level. Nephrol Dial Transplant 1996;11:1318-21.
44. Kawai M, de Paula FJ, Rosen CJ. New insights into osteoporosis: the bone-fat connection. J Intern Med 2012;272:317-29.
45. Lecka-Czernik B, Baroi S, Stechschulte LA, et al. Marrow fat-a new target to treat bone diseases? Curr Osteoporos Rep 2018;16:123-9.
46. Hardouin P, Marie PJ, Rosen CJ. New insights into bone marrow adipocytes: Report from the first European meeting on bone marrow adiposity (BMA 2015). Bone 2016;93:212-5.
47. Shoshani O, Zipori D. Transition of endothelium to cartilage and bone. Cell Stem Cell 2011;8:10-11.
48. Lin SC, Lee YC, Yu G, et al. Endothelial-to-osteoblast conversion generates osteoblastic metastasis of prostate cancer. Dev Cell 2017;41:467-480.e3.
49. Wu M, Zhang JD, Tang RN, et al. Elevated PTH induces endothelial-to-chondrogenic transition in aortic endothelial cells. Am J Physiol Renal Physiol 2017;312:F436-44.
50. Rickard DJ, Wang FL, Rodriguez-Rojas AM, et al. Intermittent treatment with parathyroid hormone (PTH) as well as a non-peptide small molecule agonist of the PTH1 receptor inhibits adipocyte differentiation in human bone marrow stromal cells. Bone 2006;39:1361-72.
51. Fan Y, Hanai JI, Le PT, et al. Parathyroid hormone directs bone marrow mesenchymal cell fate. Cell Metab 2017;25:661-72.

Cite this article as: Ni LH, Tang RN, Yuan C, Song KY, Wang LT, Zhang XL, Lv LL, Wang B, Wu M, Tang TT, Li ZL, Yin D, Cao JY, Wang XC, Liu H, Chen Q, Liu BC. Cinacalcet attenuated bone loss via inhibiting parathyroid hormone-induced endothelial-to-adipocyte transition in chronic kidney disease rats. Ann Transl Med 2019;7(14):312. doi: 10.21037/atm.2019.06.44

